Kinetics and Yields of Electron Transfer in the Inverted Region

V. Gladkikh and A. I. Burshtein*

Weizmann Institute of Science, Rehovot 76100, Israel

G. Angulo

Graz University of Technology, Graz, Austria

Stéphane Pagès, Bernard Lang, and Eric Vauthey

Department Physical Chemistry, University of Geneva, Geneva, Switzerland

Received: February 18, 2004; In Final Form: May 21, 2004

The fluorescence dynamics of perylene in the presence of tetracyanoethylene in acetonitrile was studied experimentally and theoretically, taking into consideration that the quenching is carried out by remote electron transfer in the Marcus inverted region. The initial stage was understood as a convolution of the pumping pulse with the system response accounting for the fastest (kinetic) electron transfer accompanied by vibrational relaxation. The subsequent development of the process was analyzed with differential encounter theory using different models of transfer rates distinguished by their mean square values. The single channel transfer having a bell-shaped rate with a maximum shifted far from the contact produces the ground state ion pair. It was recognized as inappropriate for fitting the quenching kinetics at moderate and long times equally well. A good fit was reached when an additional near contact quenching is switched on, to account for the parallel electron transfer to the electronically excited state of the same pair. The concentration dependence of the fluorescence quantum yield is well fitted using the same rates of distant transfer as for quenching kinetics while the contact approximation applied to the same data was shown to be inadequate.

I. Introduction

Fluorescence quenching in solutions is often considered within the classical theory of Smoluchowski[1] and Collins & Kimball,[2] assuming that the reaction is carried out at the closest approach distance between excited energy donor D* and acceptor A. This popular contact model applied to numerous systems[3] is reasonable for proton transfer[4] but bad for the long-range energy transfer governed by multipole interactions.[5−7] The electron transfer is intermediate between these two extremes. If the reaction occurs in the normal Marcus region, it can be considered as contact at fast diffusion, but at slow diffusion the effective quenching radius significantly exceeds the contact distance.[3,8,9] In the inverted region, the electron transfer is remote at any diffusion because the maximum of the Marcus rate is shifted out of contact.[3,10,11] In general, the ionization carried out by the position dependent rate $W_I(r)$ is represented by the following reaction scheme:[8]

$$\begin{array}{l} \mathrm{D}^* + \mathrm{A} \xrightarrow{W_I} \mathrm{D}^+ + \mathrm{A}^- \\ \downarrow \tau_D \end{array} \qquad (1.1)$$

The remote transfer in liquids assisted by the encounter diffusion of partners is well described by the differential encounter theory (DET)[12−17] recently reviewed in ref 3. However, for a long time the attempts to describe the reaction kinetics with either contact theory or DET were either unsuccessful or led to the nonphysical values of the electron-transfer parameters.

For instance, Fleming et al. studied the diffusion-influenced quenching reaction between rhodamine B and ferrocyanide and came to the conclusion that the Collins and Kimball contact model cannot consistently explain both the rapid initial decay (upconversion data) and the slower decay investigated with time-correlated single photon counting.[18] The fitting parameters of the model which are good for short times are poor for long-time decay and vice versa. This deficiency is inherent in the contact approximation which completely ignores the static quenching, preceding the diffusional one. Finally, it was widely recognized that "as long as we adopt realistic values of diffusion coefficients, the experimentally obtained decay curves...cannot be satisfactorily reproduced by the Collins and Kimball model, whatever values of the parameters are assumed".[19]

Calculations of this sort were also done with the rectangular[20,24] and exponential[21−23] models of the electron-transfer rate $W_I(r)$. In the normal Marcus region, the rectangular model with varying parameters is a bit better than the contact one, as well as the exponential model,

$$W_I(r) = W_c \exp\left(-\frac{2(r-\sigma)}{l}\right) \qquad (1.2)$$

which is the rough simplification of the single channel Marcus rate:

$$W_I(r) = \frac{V_0^2}{\hbar}\exp\left(-\frac{2(r-\sigma)}{L}\right)\frac{\sqrt{\pi}}{\sqrt{\lambda T}}\exp\left(-\frac{(\Delta G_I+\lambda)^2}{4\lambda T}\right)$$
$$= U(r)\mathrm{e}^{-(\Delta G_I+\lambda)^2/4\lambda T} \qquad (1.3)$$

Here V_0 and L are the contact matrix element and the length of the electron tunneling, while $\lambda(r)$ and $\Delta G_I(r)$ are the reorganiza-

10.1021/jp0492669 CCC: $27.50
Published on Web 07/10/2004

tion and free energies of ionization, T is the temperature in energy units ($k_B = 1$), and σ is the closest approach distance. Unfortunately, the very first fitting of the exponential model to the transfer kinetics also led to confusion. It was done by studying the quenching of excited pheophytin *a* by toluquinone in solvents of different viscosity.[25] The best fit for these data was obtained at $W_c = 1.8 \times 10^{10}$ s^{-1}, $\sigma = 4$ Å, and $l = 5.4$ Å. This value of l is abnormally large, not to mention L that should be even twice as large.[8]

The Marcus rate (1.3) was also used for fitting the entire quenching kinetics, but the authors failed to find the unique values of two fitting parameters, V_0 and L, in low viscosity solvents.[19] Only for high viscosity ethylene glycol they were able to fix reasonable values, but the choice of ethylene glycol was inappropriate for the reasons presented in ref 26 and confirmed later.[8] To reduce the number of parameters, L was arbitrarily put as 2 Å in ref 27 since this is "a value usually admitted in the literature". Such a choice allowed the authors to fit closely the transient quenching kinetics with rather small $V_0 = 6 \div 7$ meV.

However, the first successful attempt to estimate l from an unconditional fitting of the theory with an exponential rate to the real data was accomplished only recently.[8] The progress in experimental techniques made possible much more accurate investigation of the electron transfer between excited rhodamine 3B in the excited state and *N*,*N*-dimethylaniline in the normal Marcus region. It was studied in seven solvents of different viscosities.[28] The theoretical interpretation of the results was based on the analysis of quenching kinetics that obeys the universal asymptotic law:

$$\ln P = -c[4\pi R_Q D t + 8 R_Q{}^2 \sqrt{\pi D t}] \quad \text{at } t \to \infty \qquad (1.4)$$

where D is the coefficient of encounter diffusion, R_Q is the effective quenching radius, and

$$P(t) = N(t, c)/N(t, 0) = R(t) \exp(t/\tau_D) \qquad (1.5)$$

is the ratio of excitation populations with and without quenchers: $N(t, c)$ and $N(t, 0) = N(0) \exp(-t/\tau_D)$. The last term in eq 1.4 contributes to the nonstationary (transient) kinetics, which is not negligible over all times studied experimentally. The significant overestimation of R_Q as well as l in ref 25 resulted from ignoring this very term in the course of the fitting.

The proper extraction of R_Q from the experimental data, made in ref 8, allowed authors to fit the quasicontact and exponential models to the diffusional dependence $R_Q(D)$ getting from it a reasonable value of $l = 0.85$ Å.[8] Later a similar asymptotic analysis of transfer kinetics was employed to perylene quenched by *N*,*N*′-dimethyl-aniline in a dimethyl sulfoxide (DMSO)−glycerol mixture whose viscosity changes with composition.[29] Varying only l it was found from the best fit: $l = 0.81$ Å, $W_c = 29.12$ ns^{-1}. The transfer in this system also proceeds at relatively small $\Delta G_I < \lambda$, that is in the normal Marcus region. There $W_I(r)$ monotonically decreases with distance and can be modeled with the exponential function of eq 1.2.[3]

Here we at first turn to a reaction in the inverted region carried out by a strong electron acceptor, tetracyanoethylene (TCNE). The latter allowed Rehm and Weller to get the most exergonic points of their famous plot, although with other fluorophores.[30] The quenching of perylene (the lifetime τ_D measured after argon bubbling is 4.34 ns in our experiments) also occurs deeply in the inverted Marcus region where $\Delta G_I(\sigma) > \lambda(\sigma)$. At so high an exergonicity, $W_I(r)$ given by eq 1.3 passes through the maximum shifted out of contact,[3] so that even in the kinetic limit the reaction is remote, not to mention the diffusion-controlled ionization. However, we will demonstrate that the fitting of the experimental data with only this bell-shaped rate is impossible but becomes plausible if additional near contact quenching is added.

The origin of such an additional quenching may be attributed to parallel electron transfer to the excited state of a cation radical as suggested in ref 30. This transfer is much less exergonic and therefore occurs in the normal Marcus region, near the contact:

$$D^* + A \begin{matrix} \nearrow (\dot{D}^+)^* + \dot{A}^- \\ \searrow \dot{D}^+ + \dot{A}^- \end{matrix} \qquad (1.6)$$

Alternatively, one can consider the multichannel transfer to numerous vibronic sublevels of the ground electronic state of the ion radicals. The total rate of their production through all the vibronic channels is broader and located closer to the contact than the rate (1.3):[3,31,32]

$$W_I(r) = U(r) \sum_0^\infty e^{-S} \frac{S^n}{n!} \exp\left[-\frac{(\Delta G_I + \lambda + \hbar\omega n)^2}{4\lambda T}\right] \qquad (1.7)$$

where $S = \lambda_q/\hbar\omega$, while ω is the frequency and λ_q is the reorganization energy of the quantum vibration. Since there is no straight evidence in favor of one of these two possibilities we will sequentially consider both of them.

In fitting the real data, provision should be made for saturation of the ionization rate at short distances. There the tunneling can be so fast that the limiting stage becomes the diffusional motion along the reaction coordinate to the crossing point.[33,34] In polar solvents, this is the so-called "dynamical solvent effect" limited by the longitudinal relaxation of polarization.[35] Taking into account this effect the single channel rate takes the following form:[36,37]

$$W_I(r) = \frac{U(r)}{1 + U(r)\tau} e^{-(\Delta G_I + \lambda)^2/4\lambda T} = W_0 e^{-(\Delta G_I + \lambda)^2/4\lambda T} \qquad (1.8)$$

The upper limit of the rate, τ^{-1}, is different for activationless ($\Delta G_I = 0$)[33] and highly activated reactions ($\Delta G_I \gg T$),[35] but we will use the interpolation, which is reasonable between these two limits where most of our experimental data falls:[38]

$$\frac{1}{\tau} = \frac{1}{4\tau_L}\sqrt{\frac{\lambda}{\pi T}} \qquad (1.9)$$

Here τ_L is the longitudinal relaxation time of the solvent polarization, which assists the electron transfer. For the multiphonon rate (1.7), the generalization is straightforward:

$$W_I(r) = \sum_0^\infty \frac{U(r) e^{-S} S^n}{n! + U(r)\tau e^{-S} S^n} \exp\left[-\frac{(\Delta G_I + \lambda + \hbar\omega n)^2}{4\lambda T}\right] \qquad (1.10)$$

The saturation effect establishes the upper limit for the Arrhenius pre-exponent W_0, which is lower, the slower the dielectric relaxation. In Figure 1 we demonstrate how this limit is reached for a few solvents whose $1/\tau_L$ values were tabulated in ref 39. At the shortest interparticle distances all the curves are significantly lower than the tunneling rate, $U(r)$, especially those with long τ_L. This difference strongly reduces the total rate of

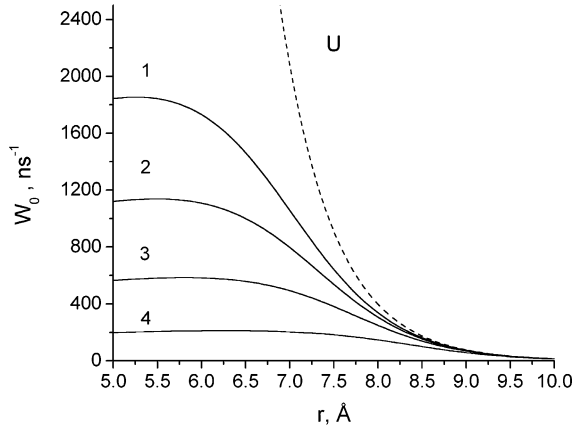

Figure 1. The Arrhenius pre-exponent as a function of distance for four solvents with different $1/\tau_L$ values: (1) acetonitrile (2.0 ps^{-1}), (2) acetone (1.2 ps^{-1}), (3) methyl acetate (0.6 ps^{-1}), (4) benzonitrile (0.21 ps^{-1}). Other parameters: $\lambda_0 = 1.15$ eV; $V_0 = 62$ meV; $\sigma = 5$ Å.

activated electron transfer $W_I(r)$, which is monotonic in the normal Marcus region (Figure 2A) and has the bell shape in the inverted one (Figure 2B).

The outline of this article is as follows. In the next section, the general formalism of DET will be briefly outlined. In section III the short, moderate, and long-time kinetics will be fitted sequentially with single-channel, double-channel, and multichannel models. In section IV, the experimental dependencies of the product quantum yields on quencher concentration will be compared with the theoretical ones specified with the transfer parameters obtained from the best fit to the kinetic data. In section V, we calculate with the same parameters the concentration dependence of the quantum yields of all the products of ionization. The results obtained are summarized in Conclusions.

II. Differential Encounter Theory of the Phenomenon

In the DET developed in refs 12−17 and reviewed in ref 3 the quenching kinetics is given by the general expression

$$R(t) = \exp(-t/\tau_D - c\int_0^t k_I(t')\,dt') \qquad (2.1)$$

where the time dependent rate constant is

$$k_I(t) = \int W_I(r) n(r, t)\, d^3r \qquad (2.2)$$

The pair correlation function $n(r, t)$ takes into account that the remote transfer running with the rate $W_I(r)$ is accelerated by the encounter diffusion represented by operator $\hat{L}$:

$$\dot{n} = -W_I(r)n + \hat{L}n \qquad (2.3)$$

If there is no inter-reactant interaction then the diffusional operator $\hat{L} = D\Delta$, while the initial and the boundary conditions to eq 2.3 take the following form:

$$n(r, 0) = 1 \quad \text{and} \quad \frac{\partial n}{\partial r}|_{r=\sigma} = 0 \qquad (2.4)$$

Over rather long times, the quenching is accelerated by diffusion and the corresponding asymptotic expression for the ionization rate constant acquires the following general form:

$$k_I(t) = 4\pi R_Q D\left[1 + \sqrt{\frac{R_Q^2}{\pi D t}}\right] \quad \text{at } t \to \infty \qquad (2.5)$$

By substituting expression (2.1) with this $k_I(t)$ into eq 1.5 one reproduces the asymptotic formula (1.4) successfully fitted to the long time kinetics. But at shorter times this asymptote is preceded by the static quenching with the rate constant followed from eqs 2.2 and 2.3 at $\hat{L} = D = 0$:

$$k_I(t) = \int W_I(r)\, e^{-W_I(r)t}\, d^3r = k_0 - \langle W_I^2 \rangle\, t + \cdots \qquad (2.6)$$

The quenching always starts with the maximal (kinetic) rate constant

$$k_0 = k_I(0) = \int W_I(r)\, d^3r = \langle W_I \rangle \qquad (2.7)$$

but then develops with retardation, which is the sharper, the higher is the mean square value

$$\langle W_I^2 \rangle = \int W_I^2(r)\, d^3r \qquad (2.8)$$

The asymptotic analysis based on eq 2.5 or (1.4) is determined by the universal parameter R_Q defined by the far periphery of $W_I(r)$ exponentially decreasing with distance. It can be approximately found from the equation:[40]

$$W_I(R_Q)l^2/D = 1$$

which is not sensitive to that part of $W_I(r)$ which is deeply inside the quenching sphere of radius R_Q. On the contrary, the static quenching starts from the maximal values of $W_I(r)$ and lasts until all the interior of the quenching sphere is burned. To discriminate between the different models of $W_I(r)$ the strategy of fitting employed in refs 8 and 29 should be changed. Here we will start by analyzing the static quenching and only after that the late diffusional quenching, as well as the total effect represented by the fluorescence and products quantum yields.

III. Experimental

The excited-state dynamics of perylene (Pe) has been measured by fluorescence upconversion (FU), using a setup already described in ref 41. Excitation was performed at 400 nm using the frequency-doubled output of a Kerr lens mode-locked Ti:sapphire laser (Tsunami, Spectra-Physics). The full width at half-maximum of the instrument response function was 210 fs.

Pe was recrystallized from benzene before use. TCNE was recrystallized from chlorobenzene and sublimed twice. Acetonitrile (acetonitrile, UV grade) was used as received. All the chemicals were from Fluka. The sample solutions were placed in a spinning cell with an optical path length of 0.4 mm. The absorbance of the sample at 400 nm was around 0.1, corresponding to a Pe concentration of the order of 10^{-4} M. All sample solutions were bubbled with Ar for 15−20 min before use. After the measurements, no significant sample degradation was observed.

The fluorescence dynamics of Pe in acetonitrile was measured with various TCNE concentrations: 0, 0.01, 0.08, 0.16, 0.32, and 0.64 M. The fluorescence dynamics of each solution was measured of five different time windows: 6, 35, 120, 300, and 1200 ps. To correct for any misalignment of the optical delay line and to have a signal intensity proportional to $P(t)$ from eq 1.5, the fluorescence time profiles at [TCNE] ≠ 0 were divided by the corresponding time profile at [TCNE] = 0. This procedure was performed with the data acquired in all time windows except the shortest one. The fluorescence dynamics

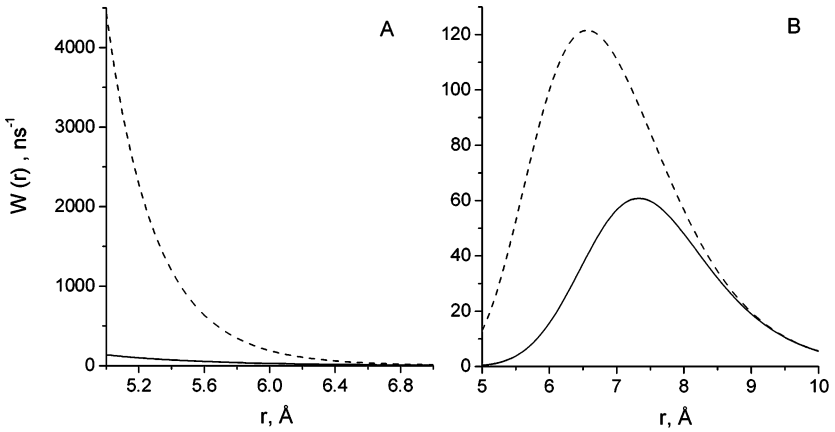

Figure 2. The ionization rates in acetonitrile with and without taking account for the transfer saturation (solid and dashed lines correspondingly). (A) Transfer in the normal Marcus region, $\Delta G_I = -0.6$ eV. (B) Transfer in the inverted Marcus region, $\Delta G_I = -2.14$ eV. The rest of the parameters are the same as in the previous figure.

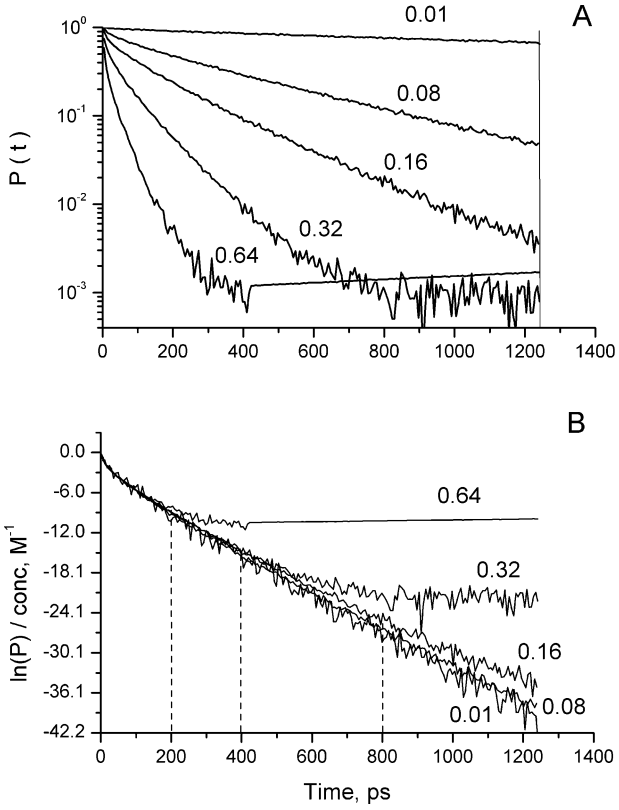

Figure 3. (A) The quenching kinetics at different concentrations of electron acceptors given in molar (numbers above curves). (B) The same but in an anamorphosis, extracting the universal time dependence of $\int_0^t k_I(t')\,dt'$. The vertical dashed lines indicate the upper borders of the credibility intervals for the highest concentrations.

was measured at 495 nm, where the effect of vibrational relaxation is the smallest, as discussed in refs 42 and 43.

IV. Fitting Kinetics of Quenching after Pulse Excitation

From the system response to the short pulse excitation in the presence and absence of quenchers, one can measure the quenching kinetics $P(t)$ given by eq 1.5. It is sharper the higher the quencher concentration used (Figure 3A), but according to the DET eq 2.1 the quantity

$$\frac{\ln P(t)}{c} = -\int_0^t k_I(t')\,dt' \tag{4.1}$$

should be the same for all concentrations. In fact, when these quantities are plotted against time all of them are practically the same for any concentrations, until they decrease (Figure 3B). However, each of them levels off approaching the level of noise. The border time between the descending branch and horizontal tail establishes the upper border of the credibility interval where the data fit the theoretical dependence (4.1). These intervals restricted by the vertical dashed lines are longer the smaller the quencher concentration. At the lowest concentrations such intervals are larger than that available for experimental study, but the depth of the reaction within the latter is small. The most suitable for fitting is the curve for $c = 0.16$ M. It reaches the same reaction depth at higher concentrations, but the integral $\int_0^t k_I(t')\,dt'$ is already as large as it is at lower concentrations. Besides, it has the lowest noise-to-signal ratio.

A. Accumulation and Dissipation of Energy at the Shortest Times. The pulse excitation to some vibrational sublevel of the upper electronic state gives way to the fast vibrational relaxation, simultaneous with the initial electron transfer. The latter proceeds with the highest (kinetic) rate constant (2.7) that allows it to compete with the vibrational relaxation. This competition can be represented by the set of model kinetic equations:

$$\dot{N}_1 = -\frac{1}{\tau_v}N_1 \quad N_1(0) = N_0 \tag{4.2a}$$

$$\dot{N} = \frac{1}{\tau_v}N_1 - ck_0N \quad N(0) = 0 \tag{4.2b}$$

where N_1 and N are the populations of initial and final (fluorescent) vibronic states, and τ_v is the vibrational relaxation time in the sub-picosecond scale. As a result, we have the following single equation for accumulation and dissipation of fluorescent particles:

$$\dot{N} = \frac{N_0}{\tau_v}\,e^{-t/\tau_v} - ck_0N \tag{4.3}$$

The solution to this equation,

$$N = \frac{N_0}{1 - ck_0\tau_v}[e^{-t/\tau_v} - e^{-ck_0t}] \tag{4.4}$$

describes both the ascending and descending branches of the initial kinetics locating the maximum between them.

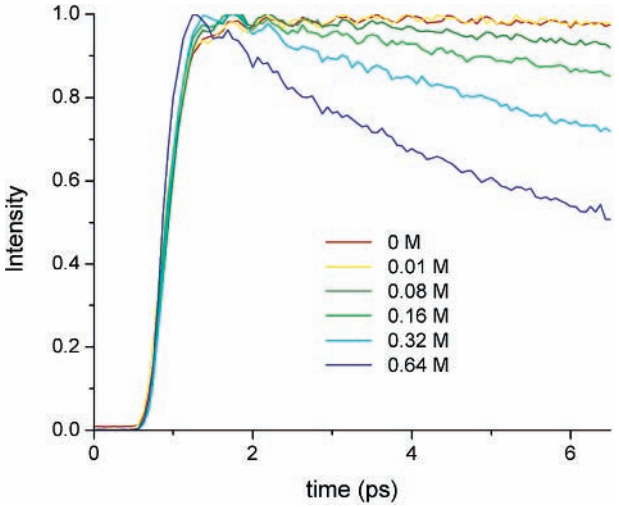

Figure 4. The FU time profiles measured with the time increment 0.062 ps at the same quencher concentrations as in the previous figure.

TABLE 1

	without convolution		with convolution	
c/M	τ_v/ps	k_0/M^{-1} ps^{-1}	τ_v/ps	k_0/M^{-1} ps^{-1}
0.08	0.282	0.20	0.215	0.25
0.16	0.257	0.20	0.200	0.22
0.32	0.255	0.20	0.186	0.23
0.64	0.183	0.20	0.119	0.21

In fact, the vibrational relaxation is not completely damped, as seen from Figure 4 which shows the fluorescence decay measured by the FU. Using the aperiodic model of vibrational relaxation (4.4) for fitting to very short data (up to 6 ps) we are looking mainly for the quenching parameter k_0 and will return back to the coherent vibrations afterward. The fitting was done in two ways: with and without convolution with the instrumental response function (IRF). They both gave similar results as shown in Table 1.

An example of the fit to the highest concentration of quenchers, $c = 0.64$ M, is given in Figure 5. It is better to include IRF in the fitting procedure, but the final values of k_0 are not affected too much. Since the further fitting of the longer time behavior will be done without convolution we set for it

$$k_0 = 0.2\ \mathrm{M}^{-1}\ \mathrm{ps}^{-1} = 322.6\ \text{Å}^3/\mathrm{ps} \qquad (4.5)$$

There is an approximately linear increase in the vibrational relaxation rate $1/\tau_v$ with quencher concentration that could be attributed to the intermolecular contribution to this rate. It can be ascribed to the vibrational energy transfer from Pe to TCNE (see Supporting Information).

B. Fitting the Moderate and Long Times with a Single-Channel Rate. If there is only the single channel of electron transfer (to the ground state of the ion pair), then in highly polar solutions the r-dependence of the ionization free energy is insignificant and according to the energy scheme of Figure 6 we have:

$$\Delta G_\mathrm{I}(r) \approx \Delta G_\mathrm{I}(\sigma) = \Delta G_i = -2.14\ \mathrm{eV}$$

The "outer-sphere" reorganization energy at contact is half at infinite separation:[3]

$$\lambda(r) = \lambda_0(2 - \sigma/r) \qquad (4.6)$$

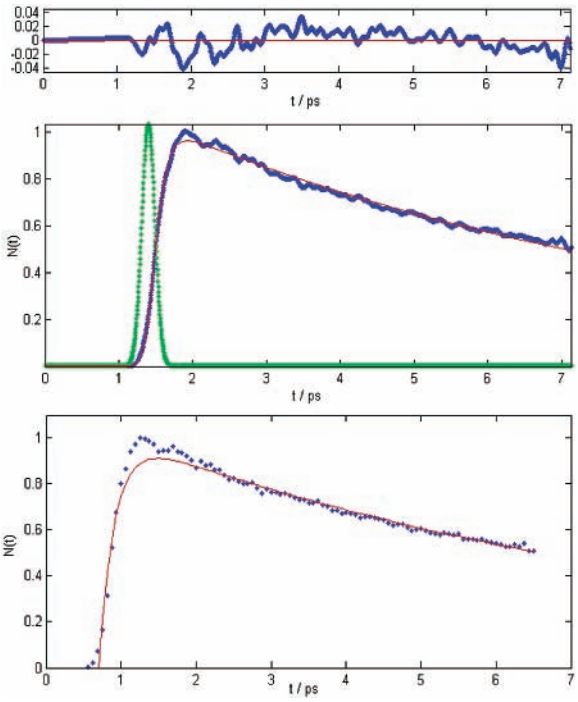

Figure 5. Fitting the very fast kinetics of accumulation and dissipation of the excited electronic state with (middle) and without (bottom) convolution with IRF. The residual of the former is shown at the top.

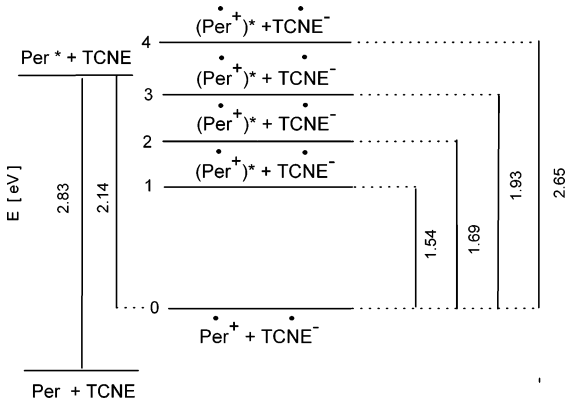

Figure 6. The energy diagram for the pair perylene + TCNE before (left) and after (right) the electron transfer.

It depends on the interparticle distance at contact σ and contact reorganization energy $\lambda_0 = \lambda(\sigma)$. In acetonitrile

$$\lambda_0 = 1.15\ \mathrm{eV}, \text{ and } \sigma = 5\ \text{Å} \qquad (4.7)$$

is an average distance between the contacting Pe and TCNE. In fact, it varies between 3.5 and 6.8 Å, depending on their coordination, but the effects of chemical anisotropy will be ignored here. Assuming a reasonable value for

$$L = 1.24\ \text{Å} \qquad (4.8)$$

we can find the remaining fitting parameter V_0 from the kinetic reaction constant (2.7), whose value is already fixed in eq 4.5. In the case of a single channel and weak transfer proceeding with the rate eq 1.3, V_0^2 is directly proportional to k_0:

$$V_0^2 = \hbar k_0 / \int \exp\left(-\frac{2(r-\sigma)}{L}\right) \frac{\sqrt{\pi}}{\sqrt{\lambda(r)T}} \exp\left(-\frac{[\Delta G_i + \lambda(r)]^2}{4\lambda(r)T}\right) \mathrm{d}^3 r$$

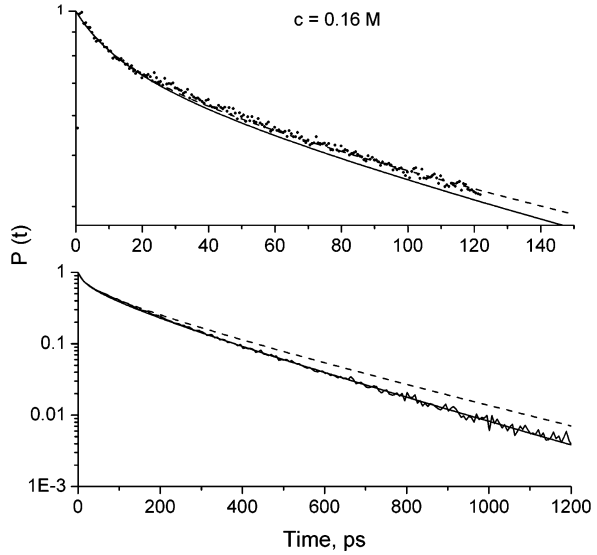

Figure 7. Fitting of single channel model to moderate (top) and long time (bottom) quenching kinetics at $c = 0.16$ M. Dashed lines obtained choosing $D = 2.45 \times 10^{-5}$ cm^2/s; solid lines represent the best fit with $D = 2.95 \times 10^{-5}$ cm^2/s ($\sigma = 5$ Å).

It follows from this relationship that

$$V_0 = 89.8 \text{ meV} \quad \text{and} \quad U_0 = \frac{V_0^2}{\hbar}\frac{\sqrt{\pi}}{\sqrt{\lambda_0 T}} = 127 \text{ ps}^{-1}$$

This value of $U_0 = U(\sigma)$ greatly exceeds the upper limit of the transfer rate established by

$$\frac{1}{\tau(\sigma)} = \frac{1}{4\tau_L}\sqrt{\frac{\lambda_0}{\pi T}} = 1.9 \text{ ps}^{-1} \tag{4.9}$$

where $\tau_L = 500$ fs (for acetonitrile). The inequality, $U\tau|_{r=\sigma} \gg 1$, clearly indicates that the saturation of electron transfer near the contact cannot be ignored.

Using the cropped transfer rate (1.8) instead of (1.3) in eq 2.7 one can find by a few iterations the appropriate V_0^2 and U_0. They appear to be larger than the previous ones to provide the same value of k_0:

$$V_0 = 138 \text{ meV} \quad \text{and} \quad U_0 = 300 \text{ ps}^{-1} \tag{4.10}$$

Using this parametrization, we tried to fit the kinetic data at moderate and long times having for our disposal only one fitting parameter: the diffusional constant D. The best results obtained for the solution with the smallest noise-to-signal ratio are shown in Figure 7. At small D, the quenching at moderate times is fitted well, but at long times is greatly underestimated. At large D, everything is quite the reverse: the quenching at long times is well approximated, but overestimated at moderate times. This is an alternative consistent with the conclusion made by Fleming et al.[18]

However, it follows unambiguously from the comparison of the short and long time results that the initial kinetic rate constant $k_0 = 322.6$ Å^3/ps is significantly larger than the final stationary rate constant

$$k_i = k_I(\infty) = 4\pi R_Q D \tag{4.11}$$

which is approximately 31.4 Å^3/ps. Such a nonstationarity of transfer is the direct indication that the quenching is under diffusion control and $k_i \approx 4\pi\sigma D \ll k_0$. This finding is in conflict with what was found when Tachiya and Murata fitted the free energy Rehm−Weller dependence of the Stern−Volmer constant that they identified with k_i.[44] According to their Figure 2, the transfer in the most exergonic systems is kinetic, that is $k_i \approx k_0$ at any time. Since our system is one of those it should be expected that $k_0 \ll k_D$ which is not the case. Being free in choosing the fitting parameters the authors made their conclusion assuming that

$$V_0 = 12.4 \text{ meV}$$

Making this choice they greatly underestimate the kinetic rate constant k_0 which is in their work 42 Å^3/ps, that is almost an order of magnitude smaller than that in eq 4.5 obtained experimentally.

Another possible cause of the discrepancy is the "closure approximation" used in this work. It is not much better than the primitive contact approximation and is especially bad in the inverted region where the transfer is essentially remote. Fortunately, this approximation is not obligatory and had been ignored in the preceding work of Marcus and Siders,[45] who applied to the similar data analysis the regular encounter theory.[15−17] They also demonstrated in their Figure 1 that at $V_0 = 4.5$ meV and $\lambda_0 = 0.56$ eV the reaction falls under kinetic control when the exergonicity of the transfer exceeds 1.5 eV. However, according to their Figure 2 the reaction remains diffusional up to $\Delta G_i = -2.2$ eV if

$$V_0 = 23 \text{ meV} \quad \text{and} \quad \lambda_0 = 0.86 \text{ eV}$$

This choice is much closer to our own although it is made for another system studied in refs 46 and 47. Marcus and Siders proposed also another way to make highly exergonic reactions diffusional, by taking into consideration the parallel transfer to the excited electronic state of the product. Until now this was a dominant idea for how to explain the too wide diffusional plateau obtained by Rehm and Weller.[3] However, it will be shown in the next subsection that the electronic excitation which occurs near the contact is much less helpful if one accounts for electron-transfer saturation which was ignored by Marcus and Siders[45] as well as by Tachiya and Murata.[44]

C. Fitting the Double-Channel Model. Looking for all possible interpretations of our data, we should take into account that the perylene cation has a number of low lying excited electronic states and at least three of them are energetically accessible from the excited reactant (Figure 6). Therefore, the formation of the cation in one of these states can compete with creation of the ground-state cation.[48−50] There are also some indications of excited ion generation in the course of highly exergonic fluorescence quenching studied in other systems: cyanoanthracene (A) and aromatic amines or aminobenzenes (D).[51,52] In all such cases there are parallel channels of ionization, to the ground state ($i = 0$) and to the excited charged products ($i = 1, 2, ...$). In our system, the transfer is exergonic to only three states. Taking them into account, one should represent the total transfer rate as a sum over parallel channels:

$$W_I(r) = \sum_{i=0}^{3} W_i(r) \tag{4.12}$$

All partial rates have the same form (1.3), but different $\Delta G_I \equiv \Delta G_i$ and tunneling matrix elements V_i. All of them contribute to the kinetic rate constant

$$k_0 = \sum_{i=0}^{3} \int W_i(r)\, \mathrm{d}^3 r = \sum_{i=0}^{3} K_i(\Delta G_i) \qquad (4.13)$$

Borrowing ΔG_i from the energetic scheme of Figure 6 we reproduced the k_0 value (4.5) with

$$V_0 = 123 \text{ meV} \quad \text{and} \quad V_i = 138 \text{ meV} \quad i = 1, 2, 3 \qquad (4.14)$$

Although tunneling to all the excited states was assumed to be equally strong their contributions to k_0 are different because of the different exergonicity of transfer.

As seen from Table 2 even at relatively high V_i the contributions from the two upper states does not exceed 3%. Therefore, they can be ignored in further investigation. Leaving only the lowest excited-state, we arrive at the double-channel model with the total rate

$$W_\mathrm{I}(r) = W_0(r) + W_1(r) \qquad (4.15)$$

where

$$W_0 = W(\Delta G_0, V_0, L) \quad \text{and} \quad W_1 = W(\Delta G_1, V_1, L)$$

are given by the general Marcus formula (1.3) but with partial arguments:

$$\Delta G_0 = -2.14 \text{ eV} \quad \text{and} \quad \Delta G_1 = -0.60 \text{ eV}$$

ΔG_1 is the free energy of transfer to the lowest excited level of perylene cation (Figure 6).[53]

In the double-channel model only V_0 and V_1 should be considered as fitting parameters. In fact, we have only a single new parameter, V_1/V_0, provided

$$k_0 = \int [W_0(r) + W_1(r)]\, \mathrm{d}^3 r \qquad (4.16)$$

is kept equal to that in eq 4.5. After finding this ratio from the best fit to the intermediate times, we adjusted also D to get the right slope of the longest quenching. The last procedure does not affect too much either the short or intermediate time behaviors which are kinetic and quasistatic in nature, that is, weakly sensitive to particle motion. At the same time, an inclusion of the excited-state production facilitates the near contact quenching, making the fitting much better, provided

$$V_0 = 123 \text{ meV} \quad V_1/V_0 = 1.12 \quad D = 3.05 \times 10^5 \text{ cm}^2/\text{s} \qquad (4.17)$$

The results shown in Figure 8 are actually much better than those achieved in Figure 7 with a single channel model.

The results of such a successful fitting allow specifying the time development of $k_\mathrm{I}(t)$ at all times, from its kinetic value, k_0, up to the stationary one, k_i (Figure 9). The slope of the $k_\mathrm{I}(t)$ dependence at $t = 0$ is the quantitative characteristic of the ln $P(t)$ curvature. It is given by the mean square rate (2.8), which is very sensitive to the shape of the particular $W_\mathrm{I}(r)$ dependence. For any remote transfer, it is finite but turns to ∞ for the contact $k_\mathrm{I}(t)$ of Collins and Kimball:

$$k_\mathrm{I}(t) = k_i^{\mathrm{con}}\left[1 + \frac{k_0}{k_\mathrm{D}} \mathrm{e}^{\alpha^2 t} \mathrm{erfc}(\alpha\sqrt{t})\right] \qquad (4.18)$$

where $k_\mathrm{D} = 4\pi\sigma D$ is the diffusional rate constant, $\alpha = \sqrt{(D/\sigma^2)(1 + (k_0/k_\mathrm{D}))}$ and

TABLE 2

channels	0	1	2	3
K_i [Å^3/ps]	273	42.3	7.21	0.211
K_i/k_0 [%]	84.6	13.1	2.23	0.07

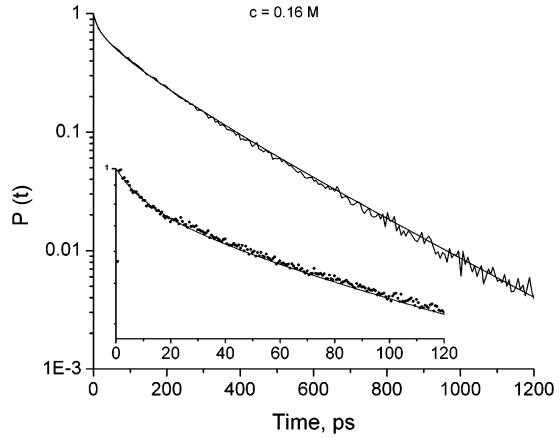

Figure 8. The fitting of the double-channel model to the quenching kinetics at $c = 0.16$ with the parameters given in eq 4.17.

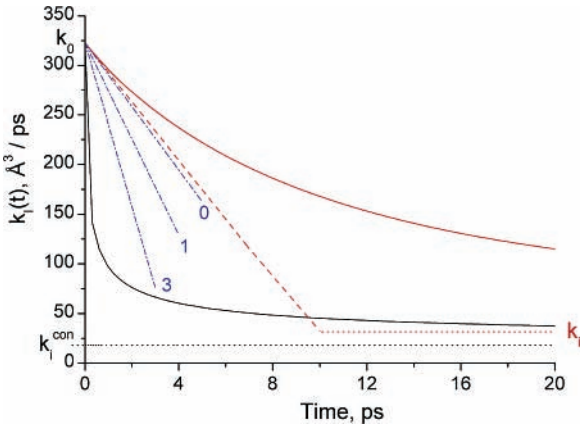

Figure 9. The double-channel "rate constant" $k_\mathrm{I}(t)$ (red line) approaching its stationary value, k_i, shown by the dotted red line. The red dashed line indicates the tangent to this curve at $t = 0$ whose absolute value is $-\dot{k}_\mathrm{I}(0) = \langle W_\mathrm{I}^2(r)\rangle$. This value for the multiphonon transfer (dashed−dotted blue lines) increases with $S = 0$, 1, 3, and turns to ∞ in the contact approximation. The latter is shown by the black line approaching its stationary value, k_i^{con} (dotted line).

$$k_i^{\mathrm{con}} = \frac{k_0 k_\mathrm{D}}{k_0 + k_\mathrm{D}} \qquad (4.19)$$

As seen from Table 3 for the double-channel model the value $|\dot{k}_\mathrm{I}(0)| = \langle W_\mathrm{I}^2\rangle$ is a bit smaller than for the single-channel model that we failed to fit well. The latter can be considered as the "zero-phonon" model ($S = 0$). In the next subsection, we will demonstrate that for the multiphonon rates ($S = 1, 2, 3, \ldots$) this quantity even increases with S, to say nothing about the contact model ($\langle W_\mathrm{I}^2\rangle = \infty$). This hierarchy is marked in Figure 9.

The double-channel rate (4.15) is composed from two components (Figure 10). The transfer saturation by the dynamic solvent effect reduces mainly the near contact one, which is responsible for the transfer to the excited state. The relative contribution of this component into $\langle W_\mathrm{I}^2\rangle$ is even smaller due to the statistical weight $4\pi r^2$. Conversely, the role of another component responsible for the transfer to the ground state is dominant and more the further it is from the contact. At relatively slow diffusion, the outer branch of this component

TABLE 3

$c = 0.16$ M	double-channel	single-channel
V_0 (meV)	123	138
V_1/V_0	1.12	0
$\langle W_I^2 \rangle$ (Å^3/ps^2)	29.6	32
$D \times 10^5$ (cm^2/s)	3.05	2.45 ÷ 2.95
R_Q (Å)	8.25	
$k_i = 4\pi R_Q D$ (Å^3/ps)	31.6	
$k_D = 4\pi\sigma D$ (Å^3/ps)	19.2	

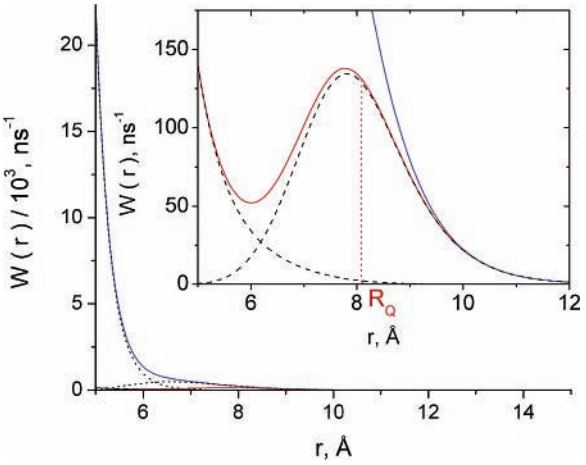

Figure 10. The rates of double-channel electron transfer with (red) and without (blue) tunneling saturation ("dynamic solvent effect"). Their components (the rates of tunneling to the ground and excited ion states) are shown by the dashed lines. The vertical dotted line indicates the quenching radii, R_Q.

determines the quenching radius R_Q, as well as the long-time asymptote of the rate constant (2.5) expressed through it.

It is of interest to compare the true value of $k_i = k_I(\infty)$ with its contact estimate (4.19). Using k_D from Table 3 we have

$$k_i^{con} = 18.1 \text{ Å}^3/\text{ps} = 0.94\, k_D = 0.056\, k_0 \qquad (4.20)$$

These results clearly indicate that the ionization is very close to the diffusional limit and rather far from the kinetic limit. In the latter case, $k(t) \equiv k_0$ should be the horizontal line shown in the same plot. The deep reduction of the rate constant with time is the clear manifestation of diffusional control over ionization. On the other hand, under diffusional control one always has $R_Q > \sigma$ and $k_i > k_i^{con}$. According to Table 3, R_Q and k_i are almost twice as much as σ and k_i^{con}.

D. Fitting the Multiphonon Model. There are at least four candidates for assistance of the electron transfer: two modes of Pe: 800 and 3100 cm^{-1}, and two of TCNE: 1100 and 2200 cm^{-1} (see Figure 2S, Supporting Information). Choosing the low-frequency ones, we compared in Figure 11 their shapes at different electron−phonon interaction measured by parameter S of the multiphonon rate (1.10). All of them are normalized to $k_0 = \int W_I(r)\, d^3r$. This value is fixed by eq. 4.5 while the rest of characteristics change with S. The general conclusion is that with growing S the rate maximum increases and shifts toward the contact. Approaching the contact is faster at a larger frequency of the assisting mode. At $\omega = 1100$ cm^{-1} the rate maximum disappears at $S = 3$ and the quenching, proceeding with quasiexponential $W_I(r)$, is maximal at the contact. Figure 12 demonstrates that $\langle W_I^2 \rangle$ monotonically increases with S and the sharper, the higher the frequency of the assisting mode. For the lowest two modes $\langle W_I^2 \rangle$ grows almost linearly with S.

At $S = 0$ any multiphonon rate reduces to a single-channel one which has the minimal $\langle W_I^2 \rangle = 32$ Å^3/ps^2. At larger S the multiphonon rates are placed between the latter and the contact one which has $\langle W_I^2 \rangle = \infty$ (see Figure 9). Therefore, in fitting our data all multiphonon models are worse than the single-channel one, let alone the double-channel model whose $\langle W_I^2 \rangle = 29.6$ Å^3/ps^2 due to the most uniform rate distribution between σ and R_Q. Judging from this criterion, we conclude that the double-channel model provides the ultimate explanation of the transient kinetics obtained in our system.

Nonetheless, it is worthy of notice that the first experimental evidence of the diffusional transfer at high exergonicity was obtained by direct study of transient effects[54] fitted with the multiphonon model. The obtained kinetic rate constants $k_0 \approx 10^{11}-10^{12}$ M^{-1}s^{-1} were shown to be much larger than diffusional ones (2×10^{10} M^{-1} s^{-1}) all over the Rehm−Weller plateau, up to $\Delta G_i = -2.2$ eV. The attempts to explain this fact theoretically were undertaken using the Collins and Kimball contact approximation.[54,55] Since $\langle W_I^2 \rangle = \infty$ in this approximation, the transient kinetics could not be well reproduced. This was not recognized as a significant drawback because the measurements on the nanosecond time scale did not allow one to study the kinetics in all the details, as we did. The disadvantage of the contact approximation manifested itself only in the diffusion control limit. There the stationary rate constants calculated with eq 4.19 were systematically smaller than the real ones: $k_D = 4\pi\sigma D < 4\pi R_Q D$.

Although both the transfer kinetics and the stationary rate constant k_i were fitted in refs 54 and 55 with the classical contact model, the single parameter of this model, k_0, was calculated using in eq 2.7 an essentially noncontact $W_I(r)$.[55] In this way, the authors carefully accounted for not only multiphonon transfer, but also for the dynamic solvent effect taking

$$\frac{1}{\tau} = 5 \text{ ps}^{-1} \quad \omega = 800 \text{ cm}^{-1} \quad S = 3$$

The upper limit for the rate ($1/\tau$) as well as ω are almost the same as ours while S is surprisingly large. Since the authors did not care about the $\langle W_I^2 \rangle$ values they admitted this choice.

But the most important difference results from the intention to stretch the region where k_0 is larger than k_D, up to the highest exergonicity of transfer. To do this Kakitani et al. revised the common definition of the reorganization energy space dependence, presenting it in the following form:

$$\lambda(r) = \Lambda(2 - \Sigma/r) \quad \text{at } r > \sigma = 4.4 \text{ Å} \qquad (4.21)$$

Considering Λ and Σ as fitting parameters they found for them the following values:

$$\Lambda = 1.35 \text{ eV} \quad \text{and} \quad \Sigma = 7.2 \text{ Å} \qquad (4.22)$$

Both of them are noticeably larger than their analogues (4.7) obtained from the available experimental data. Especially surprising is that $\Sigma > \sigma$. This relationship allows $\lambda(r)$ to vary from 0.49 eV at contact, to 2.7 eV at infinite separation, while the conventional formula (4.6) allows one only to double the minimal value.

Such an unphysical stretching of $\lambda(r)$ was taken but not for the best fit of the high exergonicity transfer. As we ensured, it can be done without any variation of the conventional space dependence of λ, eq 4.6. The stretching was necessary to fit with the same theory, the ascending branch of the Rehm−Weller free energy dependence, where the transfer is endergonic ($\Delta G_i > 0$). In fact, the same objective was also pursued by other authors cited above.[44,45] Unfortunately, it is unattainable. DET used by all of them does not hold at $\Delta G_i \gtrsim 0$. DET is good for

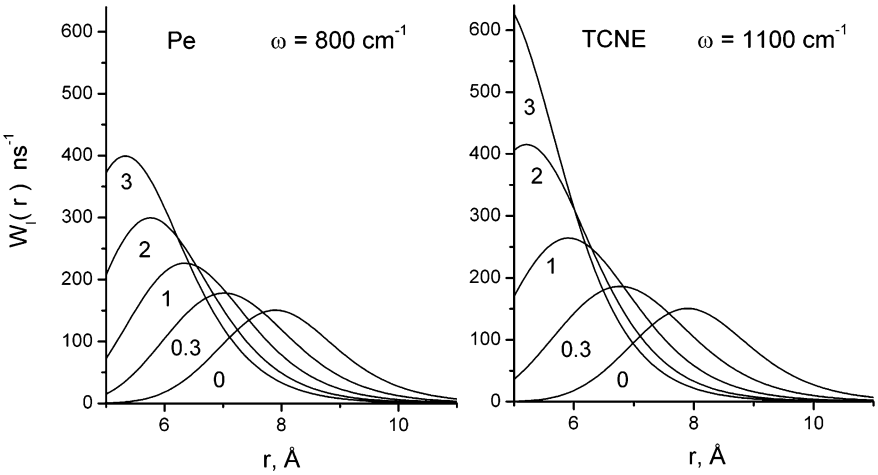

Figure 11. The rates of transfer accompanied by the vibrational excitation of Pe (left) or TCNE (right) at different $S = 0$, 0.3, 1, 2, 3 in comparison with single channel rate ($S = 0$).

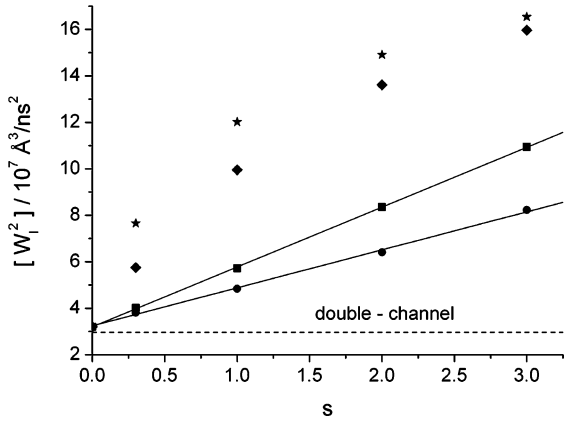

Figure 12. The S-dependence of $\langle W_l^2 \rangle$ for the quantum modes of Pe (●, 800 cm^{-1} and ★, 3100 cm^{-1}), and TCNE, (■, 1100 cm^{-1} and ◆, 2200 cm^{-1}).

high exergonicity ($-\Delta G_i \gg T$) when the backward transfer from ion pair to initial excited state is negligible, but DET is incapable of accounting for the reversible electron transfer between the excited reactants.[56] Accounting for the backward transfer requires a fundamentally different technique known as integral encounter theory (IET). It was employed for the ascending (endergonic) branch of Rehm−Weller dependence in a few recent works.[57,58] As was shown, not only the shape but the very position of the ascending branch depends on the relative strength of the radical ion pair recombination (after spin conversion in the cage or in the bulk) to either the starting excitation or excited triplet product. The rate of the latter determines the position of the ascending branch which is different for different families of the reactants. This was called the "multiple Rehm−Weller plot" in ref 59 where it was observed experimentally. At least "two different plots were clearly observed corresponding to the aromatic and olefinic compounds". This proves that fitting the data for particular systems, endergonic or exergonic, is preferable to trying to find a unique explanation for all of them together.

V. Concentration Dependence of the Stern−Volmer Constant. The relative quantum yield of the fluorescence is generally defined through the system response to instantaneous excitation (1.5) and presented in the form of the Stern−Volmer law:[3]

$$\eta = \frac{\int_0^\infty N(t, c)\,\mathrm{d}t}{\int_0^\infty N(t, 0)\,\mathrm{d}t} = \frac{1}{\tau_D}\int_0^\infty P(t)\,\mathrm{e}^{-t/\tau_D}\,\mathrm{d}t = \frac{\tilde{R}(0)}{\tau_D} = \frac{1}{1 + c\kappa\tau_D} \tag{5.1}$$

Its "constant" is in fact the concentration-dependent function $\kappa(c)$, but in the limit of small concentration it follows from the concentration expansion of eq 5.1 with $R(t)$ from eq 2.1 that

$$\eta \approx 1 - c\kappa_0\tau_D$$

where

$$\kappa_0 = \frac{1}{\tau_D}\int_0^\infty \mathrm{e}^{-t/\tau_D}\,k(t)\,\mathrm{d}t \tag{5.2}$$

is an "ideal" Stern−Volmer constant. As long as $\kappa = \kappa_0 = \text{const}$ the original Stern−Volmer law

$$1/\eta = 1 + c\kappa\tau_D \tag{5.3}$$

is linear in concentration of quenchers.

However, the factual nonlinearity of eq 5.3 resulting from the $\kappa(c)$ dependence was many times demonstrated experimentally.[60−64] We also illustrate it by Figure 13. To get η one can either use the Laplace transformation of the experimental quenching kinetics $R(t)$ in eq 5.1, or employ the conventional stationary methods for the straightforward measuring of this quantity. Using both these ways, we obtained the results which are in conformity with each other and with those resulting from the best theoretical $P(t)$ obtained with the double-channel model and integrated in eq 5.1.

Unfortunately, such a conformity is just an illusion: the presentation of data in these coordinates masks the problem. It is visualized if κ is extracted from η and plotted as a function of c. As seen from Figure 14 there is a pronounced difference between the data obtained from the time-resolved (●) and the stationary (★) experiments, not to mention the accuracy of the latter which leaves much to be desired at small c. The coincidence is satisfactory only at the highest concentration where the quenching is accomplished within the credibility time interval and conversely it is the worst at the lowest concentration when the long tail remains out of the interval available experimentally (see Figure 3A). The integration within such a limited time interval is equivalent to the sudden quenching of all donors survived to the end of it. Therefore, the quenching

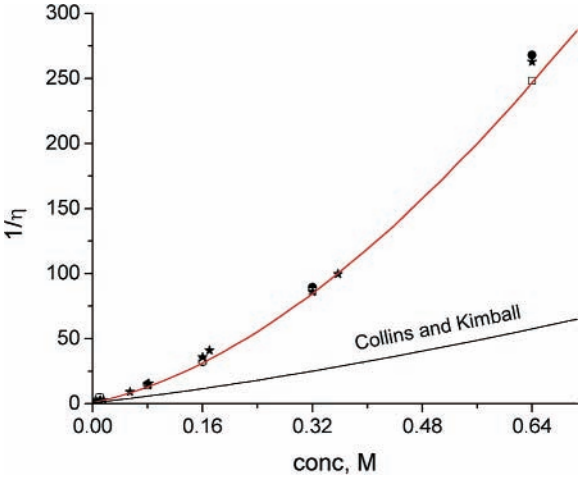

Figure 13. The nonlinear Stern−Volmer law for the quantum yield obtained by integration of the experimental quenching kinetics within the credibility intervals (●) and from the stationary measurements of the quantum yield (★). The theoretical approximation of this law with the double-channel (red line) and contact (black line) models.

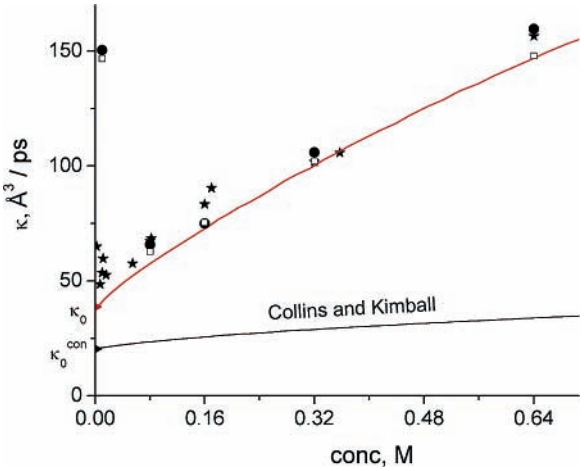

Figure 14. The Stern−Volmer constants obtained from the stationary (★) and time-resolved data (●) in comparison with the theoretical predictions, following from the double-channel quenching kinetics integrated over the credibility intervals (□) and up to infinite time (red line). Black line: the similar result but for the contact kinetics integrated over all times. Triangles (red and black): the ideal Stern−Volmer constants for the double-channel and contact models.

constant at low concentrations is greatly overestimated if $P(t)$ measured in an experimentally restricted time interval is integrated in eq 5.1.

The same is true for the theoretical κ if the integration of the model $P(t)$ in eq 5.1 is performed within the credibility time intervals (□). The coincidence of theoretical and experimental results is good for low concentration and a bit worse for the higher ones where the data are more noisy. However, it is in the range of the low concentration that the overestimation of κ takes place due to incomplete quenching within limited time interval. Fortunately, the integration of the theoretical $P(t)$ in eq 5.1 can be extended to infinity and this provides the most reliable estimate of the quantity under study (red line in Figure 14). We see that this estimate made with the double-channel model is in rather good agreement with the experimental results, unlike the contact estimate of κ (black line) obtained in the same way with the Collins-Kimball $k_I(t)$ from eq 4.18. As has been already demonstrated with Stevens data (see Figure 4 in ref 65), the contact approximation greatly underestimates the Stern−Volmer constant, and this effect increases with growing concentration. In fact, the popular contact approximation is inapplicable to electron-transfer reactions especially in the inverted region.

The main tendency established in ref 65 and seen in Figure 14 is an increase of $\kappa(c)$ from its "ideal" value $\kappa_0 = \kappa(0)$ to the maximal one: $\kappa(\infty) = k_0$. This conclusion is sustained by a number of different theoretical methods compared in ref 65. All of them except DET deal with the contact approximation ($L \rightarrow 0$). In this approximation, the ideal Stern−Volmer constant was shown to be given by the following analytic expression:[66,68]

$$\kappa_0^{con} = \frac{k_0 k_D}{k_D + k_0/(1 + \sqrt{\sigma^2/D\tau_D})} \tag{5.4}$$

Substituting into this relationship the corresponding k_0 and D values we obtain:

$$\kappa_0^{con} = 20.4\ \text{Å}^3/\text{ps} = 0.527\ \kappa_0 \tag{5.5}$$

where

$$\kappa_0 = 38.8\ \text{Å}^3/\text{ps}$$

was found from Figure 14 by extrapolation of the theoretical curve to $c = 0$. It was known for very long that in some systems even the ideal Stern−Volmer constant measured experimentally can be twice as large as its contact estimate.[67] Admitting the quenching radius R to be twice σ, the discrepancy could be understood in the framework of the extended contact theory.[67] The latter differs from the original Collins−Kimball model only by substitution of $R = \sigma/\mu$ for σ, where the numerical parameter μ can be rigorously defined through $W_I(r)$, but only near the kinetic limit ($1 - \mu \ll \mu$).[8] However, such a phenomenological extension of the contact model completely ignores the static quenching and is not applicable to true diffusional quenching ($R - \sigma \gtrsim \sigma$), especially at high concentrations.

On the contrary, the present theory accounts for remote transfer as it is. Some uncertainty is left only for the value of the tunneling length L. It may be a bit larger or smaller than $L = 1.24$ Å yet employed. The best way to eliminate such an uncertainty is to repeat the investigation in a number of solvents of different viscosities as has been done already a few times.[8,29] Varying the encounter diffusion coefficient D one can specify the $R_Q(D)$ dependence which is sensitive to the model of the transfer rate and especially to the L value.

As follows from comparison of eqs 5.4 and 4.19 $\kappa_0^{con} > k_i^{con}$ in the diffusional limit, because the Stern−Volmer constant accounts for nonstationary quenching while k_i does not. The same is true for the noncontact values of the same constants: $\kappa_0 > k_i$ (compare eqs 5.2 and 4.11). Since $\kappa(c) > \kappa_0 > k_i > k_i^{con}$ the fitting of the Rehm−Weller $\kappa(\Delta G_i)$, with the theoretically calculated $k_i(\Delta G_i)$ and especially with $k_i^{con}(\Delta G_i)$ dependence is inconsistent. Although performed in almost all published works it is incorrect in principle, but especially bad in the region of the diffusional plateau. On the other hand, the values of $\kappa(\Delta G_i)$ obtained and plotted without experimental control on quencher concentrations can differ noticeably from what they are expected to be, that is, from the ideal $\kappa_0(\Delta G_i)$ dependence.

VI. Conclusions

We present the first successful fitting of the entire kinetics of fluorescence quenching carried out by remote electron transfer

in the inverted region. Our study covers three different time scales studied with the appropriate techniques. It starts from the initial accumulation of excitations during the action of the light pulse, extends to a quasistatic electron transfer, and ends by the final quasistationary quenching.

We proved that the simplest single-channel Marcus rate, as well as its multiphonon analogues, do not allow fitting satisfactorily both the initial and the final stages of quenching. This can be done only with the double-channel model of transfer (to the ground and excited electronic state of charged products). Taking into account the saturation of the tunneling due to the dynamical solvent effect and having in hand an additional fitting parameter (the relative strength of the two channels), we fitted satisfactorily the whole kinetics of quenching. Besides, the experimentally found concentration dependence of the Stern−Volmer constant was well fitted with the same double-channel model and the same fitting parameters. Using this model, the quantum yields of the ground and excited-state products of transfer were also specified.

Two important conclusions follow from this investigation:

(i) The energy quenching by TCNE in liquid solutions is controlled by diffusion.

(ii) This is essentially distant, noncontact quenching.

These conclusions provide the unambiguous answer to the long standing question: Why is the TCNE Stern−Volmer constant placed on the diffusional plateau of the famous free energy gap law of Rehm and Weller,[30] instead of being far below it as was expected? In addition, the true value of the TCNE Stern−Volmer constant is at least twice as large as obtained in the contact approximation and this difference increases with concentration. These facts show that the contact approximation is just a convenient method of analytic calculations, but not a proper tool for fitting to the real experimental data on transfer kinetics, especially under diffusion control and at high concentrations of quenchers.

Acknowledgment. The authors are very grateful to Dr. Krissinel for the necessary perfection of the SSDP2 software package[70] and kind assistance in usage of this efficient program in our calculations. We are also grateful to Drs. D. Kattnig and A. Rosspeintner from the TU Graz for the usage of their software.

Supporting Information Available: Details of vibrational spectra and relaxation accompanied the electron transfer are presented. This material is available free of charge via the Internet at http://pubs.acs.org.

References and Notes

(1) Smoluchowski, M. V. *Z. Phys. Chem.* **1918**, *92*, 129.
(2) Collins, F. C.; Kimball, G. E. *J. Colloid Sci.* **1949**, *4*, 425.
(3) Burshtein, A. I. *Adv. Chem. Phys.* **2000**, *114*, 419.
(4) Cohen, B.; Huppert, D.; Agmon, N. *J. Phys. Chem.* **2001**, *A105*, 7165.
(5) Sveshnikov, B. Ya.; Shirokov, V. I. *Opt. Spectrosc. (USSR)* **1962**, *12*, 320.
(6) Tunitskii, N. N.; Bagdasar'yan, Kh. S. *Opt. Spectrosc. (USSR)* **1963**, *15*, 303.
(7) Yokoto, M.; Tonimoto, O. *J. Phys. Soc. Jpn.* **1967**, *22*, 779.
(8) Gladkikh, V. S.; Burshtein, A. I.; Tavernier, H. L.; Fayer, M. D. *J. Phys. Chem. A* **2002**, *106*, 6982.
(9) Neufeld, A. A.; Burshtein, A. I.; Angulo, G.; Grampp, G. *J. Chem. Phys.* **2002**, *116*, 2472.
(10) Brunchwig, B. S.; Ehrenson, S.; Sutin, N. *J. Am. Chem. Soc.* **1984**, *106*, 6859.
(11) Burshtein, A. I.; Frantsuzov, P. A.; Zharikov, A. A. *Chem. Phys.* **1991**, *155*, 91.
(12) Tunitskii, N. N.; Bagdasar'yan, Kh. S. *Opt. Spectrosc.* **1963**, *15*, 303.
(13) Kilin, S. F.; Mikhelashvili, M. S.; Rozman, I. M. *Opt. Spectrosc.* **1964**, *16*, 576.
(14) Vasil'ev, I. I.; Kirsanov, B. P.; Krongaus, V. A. *Kinet. Katal.* **1964**, *5*, 792.
(15) Steinberg I. Z.; Katchalsky, E. *J. Chem. Phys.* **1968**, *48*, 2404.
(16) Doktorov, A. B.; Burshtein, A. I. *Sov. Phys. JETP* **1975**, *41*, 671.
(17) Wilemski, G.; Fixman, M. *J. Chem. Phys.* **1973**, *58*, 4009.
(18) Eads, D. E.; Dismer, B. G.; Fleming, G. R. *J. Chem. Phys.* **1990**, *93*, 1136.
(19) Murata, S.; Matsuzaki, S. Y.; Tachiya, M. *J. Phys. Chem.* **1995**, *95*, 5354.
(20) Szabo, A. *J. Phys. Chem.* **1989**, *93*, 6929.
(21) Dorfman, R. C.; Lin, Y.; Fayer, M. D. *J. Phys. Chem.* **1990**, *94*, 8007.
(22) Song, L.; Dorfman, R. C.; Swallen, S. F.; Fayer, M. D. *J. Phys. Chem.* **1991**, *95*, 3454.
(23) Song, L.; Swallen, S. F.; Dorfman, R. C.; Weidemaier K.; Fayer M. D. *J. Phys. Chem.* **1992**, *97*, 1374.
(24) Kakitani, K.; Matsuda, N.; Denda, T.; Mataga, N.; Enomoto, Y. *Ultrafast Reaction Dynamics and Solvent Effects*; AIP Conference Proceedings 298; Gauduel, Y., Rossky, P. J, Eds., New York, 1993.
(25) Burshtein, A. I.; Kapinus, E. I.;. Kucherova, I. Yu; Morozov, V. A. *J. Luminesc.* **1989**, *43*, 291.
(26) Tavernier, H. L.; Fayer, M. D. *J. Chem. Phys.* **2001**, *114*, 4552.
(27) Allonas, X.; Jacques, P.; Accary, A.; Kessler, M.; Heisel, F. *J. Fluoresc.* **2000**, *10*, 237.
(28) Tavernier, H. L.; Kalashnikov, M. M.; Fayer, M. D. *J. Chem. Phys.* **2000**, *113*, 10191.
(29) Angulo, G.; Grampp, G.; Neufeld, A. A.; Burshtein, A. I. *J. Phys. Chem. A* **2003**, *107*, 6913.
(30) Rehm, D.; Weller, A. *Isr. J. Chem.* **1970**, *8*, 259.
(31) Efrima, S.; Bixon, M. *Chem. Phys. Lett.* **1974**, *25*, 34.
(32) Jortner, J.; Bixon, M. *J. Chem. Phys.* **1988**, *88*, 167.
(33) Burshtein, A. I.; Kofman, A. G. *Chem. Phys.* **1979**, *40*, 289.
(34) Yakobson, B. I.; Burshtein, A. I. *Chem. Phys.* **1980**, *49*, 385.
(35) Zusman, L. D. *Chem. Phys.* **1980**, *49*, 295.
(36) Burshtein, A. I.; Morozov V. A. *Chem. Phys. Lett.* **1990**, *165*, 432.
(37) Zharikov, A. A.; Burshtein, A. I. *J. Chem. Phys.* **1990**, *93*, 5573.
(38) Rips, I.; Jortner, J. *J. Chem. Phys.* **1987**, *87*, 6513.
(39) Walker, G. C.; Akesson, E.; Johnson, A. E.; Levinger, N. E.; Barbara, P. F. *J. Phys. Chem.* **1992**, *96*, 3728.
(40) Burshtein, A. I.; Doktorov, A. B.; Kipriyanov, A. A.; Morozov, V. A.; Fedorenko, S. G. *Sov. Phys. JETP* **1985**, *61*, 516.
(41) Morandeira, A.; Engeli, L.; Vauthey, E. *J. Phys. Chem. A* **2002**, *106*, 4833.
(42) Morandeira, A.; Furstenberg, A.; Gumy, J. C.; Vauthey, E. *J. Phys. Chem. A* **2003**, *107*, 5375.
(43) Pigliucci, A.; Vauthey, E. *Chimia* **2003**, *57*, 200.
(44) Tachiya, M.; Murata, S. *J. Phys. Chem.* **1992**, *96*, 8441.
(45) Marcus, R. A.; Siders, P. *J. Phys. Chem.* **1982**, *86*, 622.
(46) Creutz, C.; Sutin, N. *J. Am. Chem. Soc.* **1977**, *99*, 241.
(47) Brunschwig, B.; Sutin, N. *J. Am. Chem. Soc.* **1978**, *100*, 7568.
(48) Marcus, R. A. *J. Chem. Phys.* **1956**, *24*, 966; idem., **1965**, *43*, 679.
(49) Mataga, N.; Kanda, J.; Okada, T. *J. Phys. Chem.* **1986**, *90*, 3880.
(50) Mataga, N.; Kanda, Y.; Asahi, T.; Miyasaka, H.; Okada, T.; Kakitani, T. *Chem. Phys.* **1988**, *127*, 239.
(51) Kikuchi, K.; Katagiri, T.; Niwa, T.; Takahashi, Y.; Suzuki, T.; Ikeda, H.; Miyashi, T. *Chem. Phys. Lett.* **1992**, *193*, 155.
(52) Kikuchi, K.; Niwa, T.; Takahashi, Y.; Ikeda, H.; Miyashi, T. *J. Phys. Chem.* **1993**, *97*, 5070.
(53) Hirata, S.; Lee, T. J.; Head-Gordon M. G. *J. Chem. Phys.* **1999**, *111*, 8904.
(54) Nishikava, S.; Asahi, T.; Okada, T.; Mataga, N.; Kakitani, N. *Chem. Phys. Lett.* **1991**, *185*, 237.
(55) Kakitani, T.; Yoshimori, A.; Mataga, N. *J. Phys. Chem.* **1992**, *96*, 5385.
(56) Burshtein, A. I. *J. Lumin.* **2001**, *93*, 229.
(57) Burshtein, A. I.; Ivanov, K. L. *J. Phys. Chem. A* **2001**, *105*, 3158.
(58) Burshtein, A. I.; Ivanov, K. L. *Phys. Chem. Chem. Phys.* **2002**, *4*, 4115.
(59) Jacques, P.; Allonas, X. *J. Photochem, Photobiol. A: Chem.***1994**, *78*, 1.
(60) Nemzek, Th. L.; Ware, W. R. *J. Chem. Phys.* **1975**, *62* 479.
(61) Eftink, M. R.; Ghiron, C. R. *J. Phys. Chem.* **1975**, *80*, 486.
(62) Stevens, B.; McKeithan, D. N. *J. Photochem. Photobiol. A: Chem.* **1989**, *47*, 131.
(63) Stevens, B.; Biver, C. J., III; McKeithan, D. N. *Chem. Phys. Lett.* **1991**, *187*, 590.
(64) Stevens, B.; Biver, C. J., III *Chem. Phys. Lett.* **1994**, *226*, 268.

(65) Popov, A. V.; Gladkikh, V. S.; Burshtein, A. I. *J. Phys. Chem. A* **2003**, *107*, 8177.
(66) Lukzen, N. N.; Doktorov, A. B.; Burshtein, A. I. *Chem. Phys.* **1986**, *102*, 289.
(67) Chol, H. T.; Lipsky, S. *J. Phys. Chem.* **1981**, *85*, 4089.
(68) Burshtein, A. I.; Sivachenko, A. Y. *J. Photochem. Photobiol. A* **1997**, *109*, 1.
(69) Burshtein, A. I. *Chem. Phys. Lett.* **1992**, *194*, 247.
(70) Krissinel, E. B.; Agmon, N. *J. Comput. Chem.* **1996**, *17*, 1085.